Nonparaxial rogue waves in optical Kerr media

D. D. Estelle Temgoua[1,*] and T. C. Kofane[1,2,†]

[1]*Laboratory of Mechanics, Department of Physics, Faculty of Science, University of Yaounde I, P.O. Box 812, Yaounde, Cameroon*

[2]*Centre d'Excellence Africain en Technologies de l'Information et de la Communication, University of Yaounde I, P.O. Box 812, Yaounde, Cameroon*

(Received 1 December 2014; revised manuscript received 14 March 2015; published 3 June 2015)

We consider the inhomogeneous nonparaxial nonlinear Schrödinger (NLS) equation with varying dispersion, nonlinearity, and nonparaxiality coefficients, which governs the nonlinear wave propagation in an inhomogeneous optical fiber system. We present the similarity and Darboux transformations and for the chosen specific set of parameters and free functions, the first- and second-order rational solutions of the nonparaxial NLS equation are generated. In particular, the features of rogue waves throughout polynomial and Jacobian elliptic functions are analyzed, showing the nonparaxial effects. It is shown that the nonparaxiality increases the intensity of rogue waves by increasing the length and reducing the width simultaneously, by the way it increases their speed and penalizes interactions between them. These properties and the characteristic controllability of the nonparaxial rogue waves may give another opportunity to perform experimental realizations and potential applications in optical fibers.

DOI: 10.1103/PhysRevE.91.063201 PACS number(s): 05.45.−a, 42.65.−k, 42.25.Bs, 42.70.−a

I. INTRODUCTION

The generation of solitons in optical fibers, predicted by Hasegawa and Tappert [1] through the balance between the pulse broadening due to self-phase modulation and compression due to negative group-velocity dispersion (GVD), has enabled the generation of stable picosecond and subpicosecond pulses in the near infrared. In a weakly nonlinear dispersive medium, the dynamics of the pulse envelope is governed in the paraxial approximation by the cubic nonlinear Schrödinger (NLS) equation [1].

An important property of NLS equation solitons is that they emerge from particular initial profiles as long as a particular threshold condition is met. As a consequence, it is possible to experimentally observe solitons when neither the initial pulse amplitude nor the initial pulse shape corresponds to a pure soliton. Therefore, verification of many of the predicted soliton pulse characteristics was carried out in a series of experiments by Mollenauer and co-workers [2–4].

Temporal, spatial, and spatiotemporal optical solitons can find applications including all-optical routing, transparent beam interconnections, and the massive integration of optical operations in a fully three-dimensional environment. In fact, light is self-guiding in bulk media, which have modes with numerical apertures that violate the paraxial approximation. We recall that the paraxial approximation is valid when the radius of the beam is sufficiently large compared to the wavelength. Nonparaxiality may arise in the miniaturization of devices and in other configurations, such as those involving multiplexed beams [5]. Analytical and numerical studies of nonparaxial bright and dark solitons in optical Kerr media have been reported [6]. In particular, Barruch *et al.* [6] solved numerically the (2+1)-dimensional nonlinear Helmholtz equation for input beams that collapse in the simpler model. They used a Kerr-slab material of finite length and solved the (1+1)-dimensional nonlinear Helmholtz equation for an incoming soliton profile.

It is found that the solution inside the Kerr-slab propagates virtually unchanged and solitonlike solutions still exist even for such a narrow beam for which the nonparaxiality is still moderate. Chamorra-Posada *et al.* [7] have investigated and shown that the nonlinear Helmholtz equation, which can also be taken as the NLS equation, has an exact nonparaxial soliton solution from which the paraxial soliton is recovered in the appropriate limit. Based on the general particlelike nature of solitons, Fewo *et al.* [8] have described some physical parameters for the pulses such as the amplitude, the chirp, the frequency, and the pulse width. They derived the generalization of the matrix equation using a collective variable approach, leading to a set of second-order differential equations of motion of the nonparaxial spatial optical solitons.

The focusing NLS equation, which describes generic nonlinear phenomena, supports a whole hierarchy of recently discovered Peregrine soliton or rational solutions [9,10], Ma solitons [11], and Akhmediev breathers [12,13]. Although solitary by nature, these rational solutions or rogue waves are different from the usual solitons in that they are rare, short lived, and unstable. They can emerge from a turbulent state of random fields, while ordinary solitons are stable waves with characteristic collision properties, commonly appearing in a deterministic setting of nonlinear evolution partial differential equations. Rogue waves are giant single waves that may suddenly appear in oceans [14]. In recent years, the idea of rogue waves has been extended far beyond oceanic expanses. The concept has been applied to pulses emerging from optical fibers [10,14–22] and waves in Bose-Einstein condensates [23], in superfluids [16], in optical cavities [18], in the atmosphere [24], and even in finance [25].

In particular, rogue wave solutions emerging from optical fibers have been found analytically for many types of generalized NLS models such as NLS models with constant coefficients [10,26–29] and NLS models with varying coefficients [9,30,31]. Recently, this interesting phenomenon of optical rogue waves has been verified experimentally [21,32].

*Corresponding author: estelletemgoua@yahoo.fr

†tckofane@yahoo.com

According to the controllability of rogue waves, which has been studied before [33–38], the problem now is what waves, which are localized in both space and time and depict a unique event that appears from nowhere and disappears without a trace [39], can exist in the presence of the GVD and Kerr nonlinearity in the nonparaxial approximation.

The present paper is organized as follows. In Sec. II we use the similarity transformation and the modified Darboux transformation to investigate the analytical nonparaxial rogue wave solutions. In Sec. III we focus our attention on the effect of the nonparaxiality on the propagation of rogue waves to solve the problem of controllability of rogue waves in the nonparaxial approximation by selecting parameters of the original equation. In Sec. IV a summary is given.

II. SIMILARITY TRANSFORMATION AND RATIONAL SOLUTIONS OF THE NONPARAXIAL NONLINEAR SCHRÖDINGER EQUATION WITH VARIABLE COEFFICIENTS

The complex envelope of the optical field $\psi(z,x)$ of a continuous-wave beam liable to a linear diffraction in one transverse dimension in isotropic Kerr media moves according to the nonparaxial NLS equation in the form [8]

$$d\psi_{zz} + i\psi_z + p\psi_{xx} + q|\psi|^2\psi = 0, \tag{1}$$

where z and x are the longitudinal and transverse coordinates, respectively,

$$x = \tilde{x}/r_0, \quad z = \tilde{z}/2L_{DF}, \quad \psi = \sqrt{2n_2/n_0}r_0k_0\tilde{A}, \tag{2}$$

where r_0 is the input beam radius with diffraction length $L_{DF} = k_0r_0^2$, k_0 is the linear wave number, n_0 is the linear index of refraction, n_2 is the Kerr coefficient, $\tilde{A}(x,z)$ is unscaled field assumed to be slowly varying, and $d = \frac{1}{(r_0k_0)^2}$ is the nonparaxiality parameter. The parameters p and q are related to the GVD and Kerr nonlinearity, respectively. Equation (1) quantifies changes in the transverse profile of a light beam with respect to a forward-propagating reference frame and can be seen as the nonparaxial NLS equation. This equation has been used in the literature [6,7,40,41] for fixed values of the dimensionless parameters p and q.

In the presence of management, the optical pulse propagation in Kerr media can be described by the nonparaxial NLS equation with variable coefficients in the form

$$d(z)\psi_{zz} + i\psi_z + p(z)\psi_{xx} + q(z)|\psi|^2\psi = 0. \tag{3}$$

Here z is taken as the time parameter. The variable coefficients $d(z)$, $p(z)$, and $q(z)$, which are functions of the propagation distance z, are related to the nonparaxiality, GVD, and Kerr nonlinearity, respectively. Inspired by the previous work of Yan and Dai [42], we use the envelope field in the form

$$\psi(z,x) = \rho(z)V[Z(z),X(z,x)]\exp[i\varphi(z,x)] \tag{4}$$

to investigate the rational solutions related to nonparaxial rogue waves, where $\rho(z)$ is the amplitude, $Z(z)$ the effective propagation distance, $X(z,x)$ the similitude variable, and $V[Z(z),X(z,x)]$ the complex field. The variable $\varphi(z,x)$ is the phase of the wave. This form of the envelope field is also known as the similarity transformation or the symmetry reduction method. This method, which is also based on the self-similarity of specific partial differential equations, has been applied in NLS equations to search for the exact and the asymptotic self-similar solutions [43–45]. Equation (3) is not integrable because of varying dispersion, nonlinearity, and nonparaxiality coefficients, which govern the nonlinear wave propagation in an inhomogeneous optical fiber system. In order to construct exact analytical solutions of Eq. (3) we should reduce it to some integrable differential equation: the standard NLS equation. So in what follows we use the symmetry transformation method to obtain integrability conditions. This kind of exact analytical solution has more attractive properties than those of the soliton because of its reduced interaction and smaller peak power than that of the soliton [46] and allows a possible pedestal-free pulse compression [47]. Notice that the similarity and the modified Darboux transformation methods are analytical methods that enable us to construct rational solutions related to rogue waves.

Substituting Eq. (4) into Eq. (3) gives a couple system of partial differential equations with variable coefficients

$$\begin{aligned}&\rho_z V + 2p\rho X_x\varphi_x V_X + \rho Z_z V_Z + \rho X_z V_X + 2\rho d\varphi_z X_z V_X\\ &\quad + p\rho\varphi_{xx}V + \rho dV\varphi_{zz} + 2d\rho_z V\varphi_z + 2\rho d\varphi_z Z_z V_Z = 0,\end{aligned} \tag{5}$$

$$\begin{aligned}&d\rho_{zz}V + 2d\rho_z Z_z V_Z + 2d\rho_z X_z V_X + \rho d{Z_z}^2 V_{ZZ}\\ &\quad + 2d\rho Z_z X_z V_{ZX} + \rho d Z_{zz} V_Z + \rho d{X_z}^2 V_{XX} + d\rho X_{zz} V_X\\ &\quad - d\rho V{\varphi_z}^2 - \rho V\varphi_z + p\rho{X_x}^2 V_{XX} + p\rho X_{xx}V_x\\ &\quad - p\rho V{\varphi_x}^2 + q|\rho|^2|V|^2\rho V = 0.\end{aligned} \tag{6}$$

According to previous works [9,30], we consider the above symmetry (reduction) transformation or similarity transformation (4) that would reduce Eq. (3) to the standard NLS equation

$$i\psi_z + \tfrac{1}{2}\psi_{xx} + |\psi|^2\psi = 0. \tag{7}$$

By connecting the solutions of Eq. (3) with those of the above standard NLS equation, the complex field $V[Z(z),X(z,x)]$ should satisfy that equation in the form

$$i\frac{\partial V}{\partial Z} + \frac{1}{2}\frac{\partial^2 V}{\partial X^2} + |V|^2V = 0. \tag{8}$$

With $V[Z(z),X(z,x)]$ satisfying the relation (8), we have after the similarity reduction of Eqs. (5) and (6)

$$d(z)X_{zz} + p(z)X_{xx} = 0, \tag{9}$$

$$q(z)\rho^2 + Z_z = 0, \tag{10}$$

$$Z_z + d(z)\varphi_z Z_z = 0, \tag{11}$$

$$\tfrac{1}{2}Z_z + p(z){X_x}^2 + d(z){X_z}^2 = 0, \tag{12}$$

$$\varphi_z + d(z){\varphi_z}^2 + p(z){\varphi_x}^2 = 0, \tag{13}$$

$$\rho_z + \rho(p(z)\varphi_{xx} + d(z)\varphi_{zz}) + 2d(z)\rho_z\varphi_z = 0, \tag{14}$$

$$\begin{aligned}&\rho_{zz}V + 2\rho_z Z_z V_Z + 2\rho_z X_z V_X + \rho{Z_z}^2 V_{ZZ}\\ &\quad + 2\rho Z_z X_z V_{ZX} + \rho Z_{zz} V_Z = 0.\end{aligned} \tag{15}$$

We start the resolution of the system (9)–(15) by solving Eq. (9).

In order to look for rational solutions, several conditions are imposed,

$$Z_z = -\tfrac{1}{2}p(z){X_x}^2, \quad q(z) = \tfrac{1}{2}p(z)\rho(z)^{-2}{X_x}^2, \quad X_x = \alpha(z), \tag{16}$$

which verify Eq. (10). The above parameters can generate the constraints for the variable $Z(z)$ and the nonlinear Kerr coefficient $q(z)$. More specifically, it follows that

$$X_x = \alpha(z), \quad X_{xx} = 0. \tag{17}$$

As $d(z) \neq 0$ and $p(z) \neq 0$, Eq. (9) leads to the condition $X_{zz} = 0$, which implies that $\alpha_{zz} = \delta_{zz} = 0$. So from relations (17) we obtain

$$X(z,x) = \alpha(z)x + \delta(z), \tag{18}$$

where $\alpha(z)$ is the inverse of the wave width and $\delta(z)$ the position of its center of mass $-\delta(z)/\alpha(z)$. Quantities $\alpha(z)$ and $\delta(z)$ are free functions of z.

From condition (16) we obtain the effective dimensionless propagation distance

$$Z(z) = -\frac{1}{2}\int_0^z p(s)\alpha(s)^2 ds. \tag{19}$$

Substituting Eq. (16) into Eq. (12) leads to

$$X_z^2 = -\frac{3p(z)\alpha(z)^2}{4d(z)}. \tag{20}$$

The relation above is true for $d(z) < 0$ or $p(z) < 0$. In this work we choose $p(z) < 0$. For $Z_z \neq 0$, Eq. (11) becomes

$$\varphi_z = -\frac{1}{d(z)}. \tag{21}$$

Substituting Eq. (21) into Eq. (13), we obtain the phase expression

$$\varphi_x = 0, \quad \varphi_{xx} = 0, \quad \varphi(z,x) = -\int_0^z \frac{1}{d(s)} ds + \varphi_0(x), \tag{22}$$

where $\varphi_0(x)$ is a constant.

From Eq. (14) we have

$$\rho(z) = \rho_0 \exp\left(\int_0^z \gamma(s) ds\right), \tag{23}$$

which is the amplitude of the wave, assumed to be a real function, and where $\gamma(s)$ leads to

$$\gamma(s) = d(s)\varphi_{zz}. \tag{24}$$

Here ρ_0 is a constant. Now we can deduce the Kerr coefficient given by

$$q(z) = \frac{1}{2}\frac{p(s)\alpha(s)^2}{\rho_0^2 \exp\left(2\int_0^z \gamma(s) ds\right)}. \tag{25}$$

For the defined values of $d(z)$, $p(z)$, $\alpha(z)$, and $\delta(z)$, we can give the expressions of $X(z,x)$, $Z(z)$, $\rho(z)$, $\varphi(z,x)$, and $q(z)$.

To determine the variable $V[Z(z),X(z,x)]$, we use a dressing method of the modified Darboux transformation [26,48–50]. The first order of the standard NLS equation given by Eq. (1) was found by Peregrine [10] and the second order was proposed by Soto-Crespo *et al.* [51].

According to the modified Darboux transformation, we obtain the first and the second order of rational solutions. If we let $V[Z(z),X(z,x)] = \Psi[Z(z),X(z,x)]$, the first order presented in Refs. [9,10] is given by

$$\Psi_1 = V_1 = \left[1 - \frac{G_1 + iZ(z)H_1}{1 + 2X^2 + 4Z^2}\right] \exp i\{Z(z)\}, \tag{26}$$

where

$$G_1 = 4, \quad H_1 = 8, \quad D_1 = 1 + 2X^2 + 4Z^2. \tag{27}$$

This solution is known as the Peregrine soliton [10] when we consider the correspondence $Z = z$ and $X = x\sqrt{2}$. Then, collecting the partial solutions together, we construct the first-order rational solution related to the exact nonparaxial rogue wave solution of Eq. (3)

$$\psi_1 = \rho_0 \exp\left\{\int_0^z \gamma(s) ds\right\}\left[1 - 4\frac{1 + 2iZ(z)}{1 + 2X(z,x)^2 + 4Z(z)^2}\right] \times \exp i\{Z(z) + \varphi(z,x)\}. \tag{28}$$

The intensity of the first-order nonparaxial rogue wave is given by

$$|\psi_1|^2 = {\rho_0}^2 \exp\left\{2\int_0^z \gamma(s) ds\right\}\left(\frac{(2X^2 + 4Z^2 - 3)^2 + 64Z^2}{(1 + 2X^2 + 4Z^2)^2}\right). \tag{29}$$

This first-order rational solution is used to describe the dynamics of rogue waves in optical fibers. We use it to show the effect of the nonparaxiality on the propagation of rogue waves and present the different cases in which the choice of parameters of the original equation (3) lead to the control of rogue waves. The second-order rogue wave presented in Ref. [9] is given by

$$\Psi_2 = V_2 = \left[1 + \frac{G_2 + iZ(z)H_2}{D_2}\right] \exp i\{Z(z)\}, \tag{30}$$

where G_2, H_2, and D_2 are given by the relations

$$\begin{aligned} G_2 &= \tfrac{3}{8} - \tfrac{3}{2}X^2 - \tfrac{1}{2}X^4 - 9Z^2 - 10Z^4 - 6X^2Z^2, \\ H_2 &= \tfrac{15}{4} + 3X^2 - X^4 - 2Z^2 - 4Z^4 - 4X^2Z^2, \\ D_2 &= \tfrac{3}{32} + \tfrac{9}{16}X^2 + \tfrac{1}{8}X^4 + \tfrac{1}{12}X^6 + \tfrac{33}{8}Z^2 \\ &\quad + \tfrac{9}{2}Z^4 + \tfrac{2}{3}Z^6 - \tfrac{3}{2}X^2Z^2 + \tfrac{1}{2}X^4Z^2 + X^2Z^4. \end{aligned} \tag{31}$$

According to the same correspondence of variables z and x as for first order, this solution is the one found by Soto-Crespo *et al.* [51]. Collecting the partial solutions together, we construct the final second-order rational solution related to the exact nonparaxial rogue wave solution of Eq. (3)

$$\psi_2 = \rho_0 \exp\left\{\int_0^z \gamma(s) ds\right\}\left[1 + \frac{G_2 + iZ(z)H_2}{D_2}\right] \times \exp i\{Z(z) + \varphi(z,x)\}. \tag{32}$$

The intensity of the second-order nonparaxial rogue wave solution is

$$|\psi_2|^2 = \rho_0^2 \exp\left\{2\int_0^z \gamma(s) ds\right\}\left(\frac{(D_2 + G_2)^2 + Z^2H_2^2}{D_2^2}\right). \tag{33}$$

This second-order rational solution is more precise than the first one. It describes the dynamics of two rogue waves propagating in an optical fiber as well as collisions between them. We will use it to illustrate the effect of the nonparaxiality on rogue wave collisions.

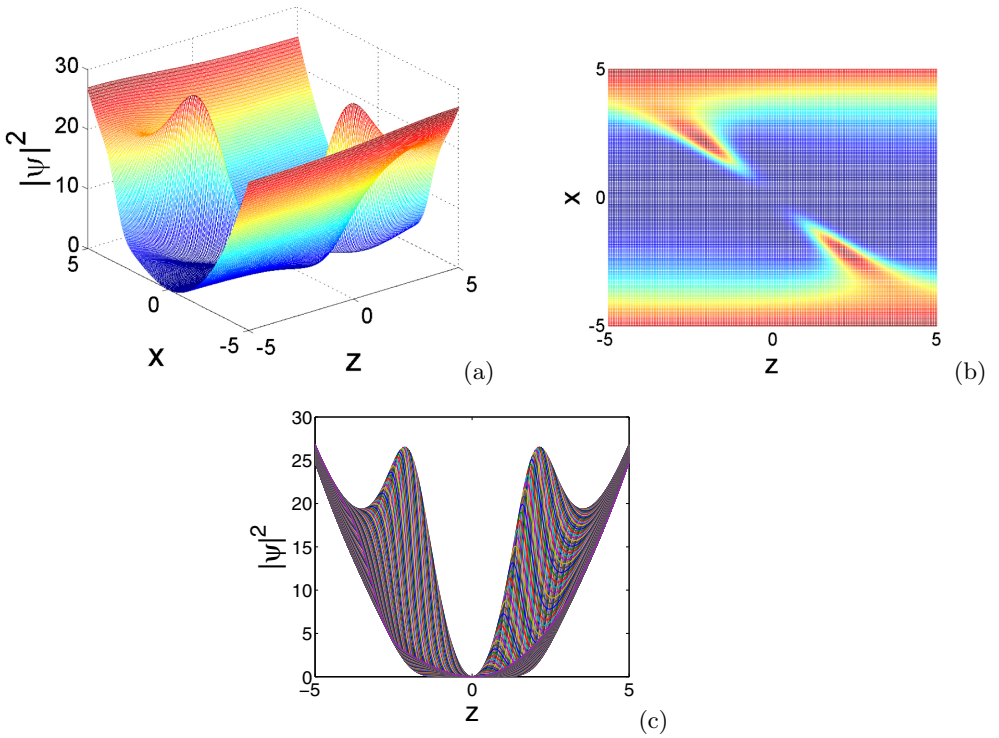

FIG. 1. (Color online) Wave propagation in 2D and 3D representations of the first-order rational solution for the intensity $|\psi_1(x,z)|^2$ with $d(z) = \frac{z}{4}$, $p(z) = -\frac{z^2}{4}$, $\alpha(z) = 1$, and $\delta(z) = z$.

III. EFFECT OF THE NONPARAXIALITY ON THE PROPAGATION OF ROGUE WAVES IN OPTICAL FIBER

To illustrate the effect of the nonparaxiality on the propagation of rogue waves related to the first- and second-order rational solutions, we fix values of parameters $\rho_0 = 1$. We present managed cases, in which the choice of parameter functions leads to the control of rogue waves.

Our goal now is to choose appropriately free functions $d(z)$, $P(z)$, $\alpha(z)$, and $\delta(z)$ so that we can generate abundant structures of nonparaxial rogue waves. We choose them as polynomial functions. We noted that parameters are chosen in order to be bounded in the intervals $-5 < z < 5$ and $-5 < x < 5$.

For the chosen coefficients and free functions

$$d(z) = \frac{z}{4}, \quad p(z) = -\frac{z^2}{4}, \quad \alpha(z) = 1, \quad \delta(z) = z. \quad (34)$$

The wave propagations is presented in Fig. 1 in three-dimensional (3D) [Fig. 1(a)] and 2D [Figs. 1(b) and 1(c)] representations showing the nonparaxial effects. For the given parameters

$$d(z) = \frac{1}{4}, \quad p(z) = -\frac{z^2}{4}, \quad \alpha(z) = 1, \quad \delta(z) = z. \quad (35)$$

Figure 2 depicts the dynamics of the first-order rational solution for the intensity $|\psi_1(x,z)|^2$ in 3D [Fig. 2(a)] and 2D [Figs. 2(b) and 2(c)] representations illustrating the nonparaxial effects on the propagation of rogue waves.

In this paper we plot the intensity of the first- and second-order rational solutions with the help of MATLAB. We can see in Figs. 1 and 2 that the behavior of the nonparaxial rogue waves is more surrounded in Fig. 1 than in Fig. 2. We observe that the space where the usual rogue waves reach their maximum moves from the center to the periphery in Fig. 1. So the usual symmetry of the Peregrine soliton is absent in Fig. 1 with the nonparaxial parameter $d(z)$ taken as the polynomial function and present in Fig. 2 with $d(z)$ taken as a constant. This means that the choice of nonparaxial parameter $d(z)$, given in relation (34), is appropriate to obtain particularities of nonparaxial effects. The intensity profile of Fig. 1 increases more rapidly than the ones of the usual cases in the paraxial approximation. It follows that the nonparaxiality increases the length and reduces the width of the wave peak simultaneously. It is also responsible for the unusual symmetry of the Peregrine soliton (rogue waves) in Fig. 1.

We first show the influence of polynomial functions $d(z)$, $p(z)$, $\alpha(z)$ and $\delta(z)$ on the structure of nonparaxial rogue waves. Second, we choose some of them now as Jacobian elliptic functions. When k is weaker than one, the approximative formulas of Jacobian elliptic functions [52] are given by

$$\begin{aligned} \mathrm{dn}(z,k) &\approx 1 - \frac{k^2 \sin(z)^2}{2}, \\ \mathrm{cn}(z,k) &\approx \cos(z) - k^2 \sin(z)\left(\frac{z - \sin(z)\cos(z)}{4}\right), \\ \mathrm{sn}(z,k) &\approx \sin(z) - k^2 \cos(z)\left(\frac{z - \sin(z)\cos(z)}{4}\right). \end{aligned} \quad (36)$$

Here we choose $k = 0.6$. If we set coefficients and free functions as

$$d(z) = \mathrm{cn}(z,k), \quad p(z) = -\tfrac{1}{2}\mathrm{sn}(k,z) \quad \alpha(z) = z, \quad \delta(z) = z, \quad (37)$$

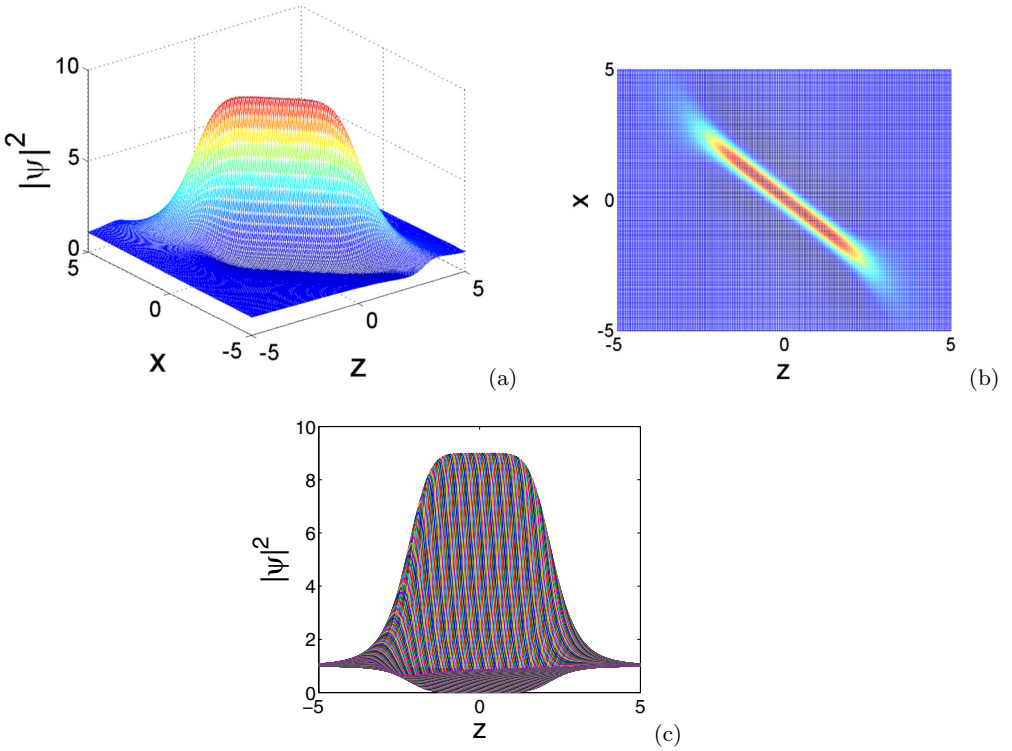

FIG. 2. (Color online) Wave propagation in 2D and 3D representations of the first-order rational solution for the intensity $|\psi_1(x,z)|^2$ with $d(z) = \frac{1}{4}$, $p(z) = -\frac{z^2}{4}$, $\alpha(z) = 1$, and $\delta(z) = z$.

we can obtain the 3D and 2D representation profiles in Figs. 3(a) and 3(c), respectively, showing the nonparaxial effects on rogue waves.

Figures 3(a)–3(c) depict the behavior of nonparaxial rogue waves with $d(z)$ and $p(z)$ taken as Jacobian elliptic functions. The profiles show waves with usual symmetry along the

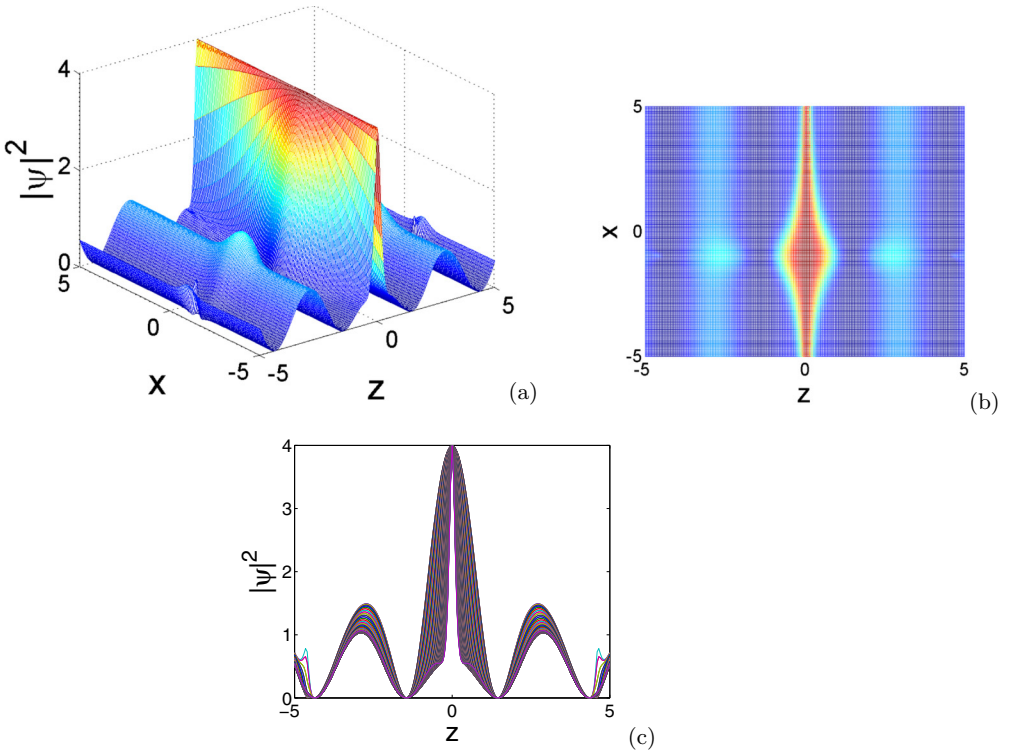

FIG. 3. (Color online) Wave propagation in 2D and 3D representations of the first-order rational solution for the intensity $|\psi_1(x,z)|^2$ with $d(z) = \mathrm{cn}(z,k)$, $p(z) = -\frac{1}{2}\mathrm{sn}(k,z)$, $\alpha(z) = z$, and $\delta(z) = z$.

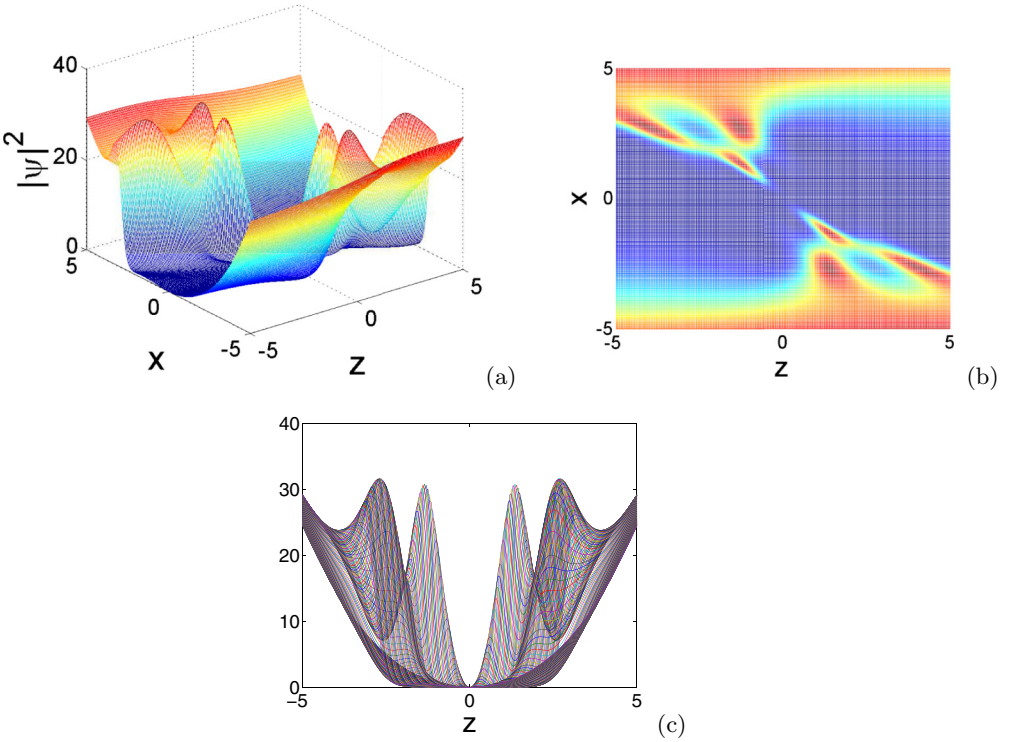

FIG. 4. (Color online) Wave propagation in 2D and 3D representations of the second-order rational solution for the intensity $|\psi_2(x,z)|^2$ with $d(z) = \frac{z}{4}$, $p(z) = -\frac{z^2}{4}$, $\alpha(z) = 1$, and $\delta(z) = z$.

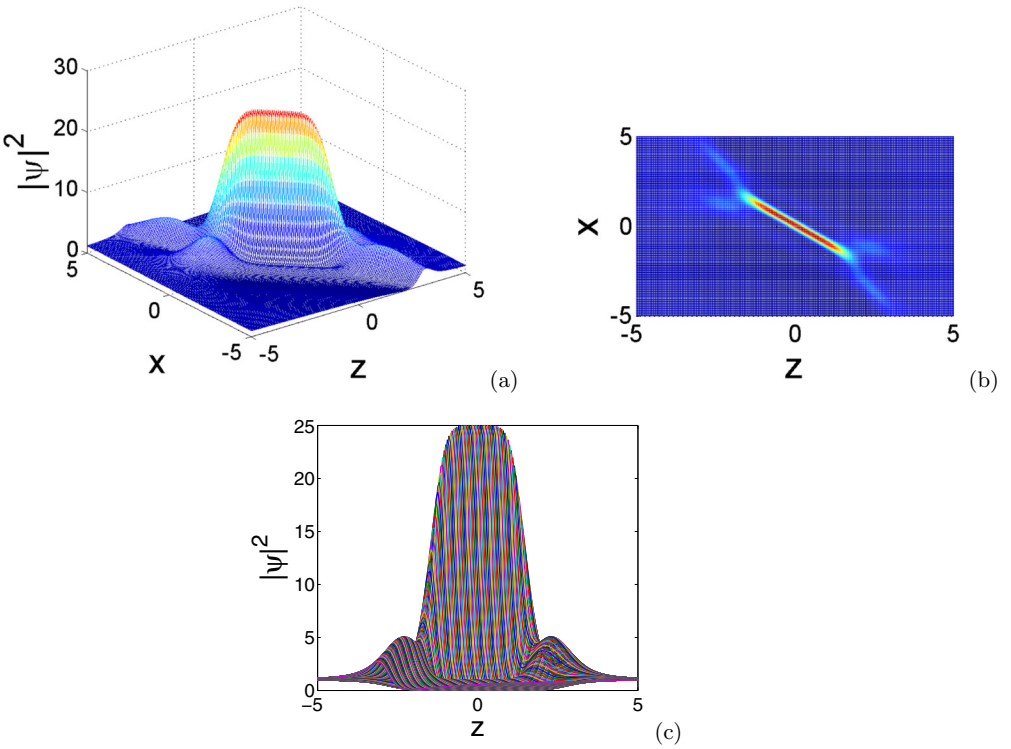

FIG. 5. (Color online) Wave propagation in 2D and 3D representations of the second-order rational solution for the intensity $|\psi_2(x,z)|^2$ with $d(z) = \frac{1}{4}$, $p(z) = -\frac{z^2}{4}$, $\alpha(z) = 1$, and $\delta(z) = z$.

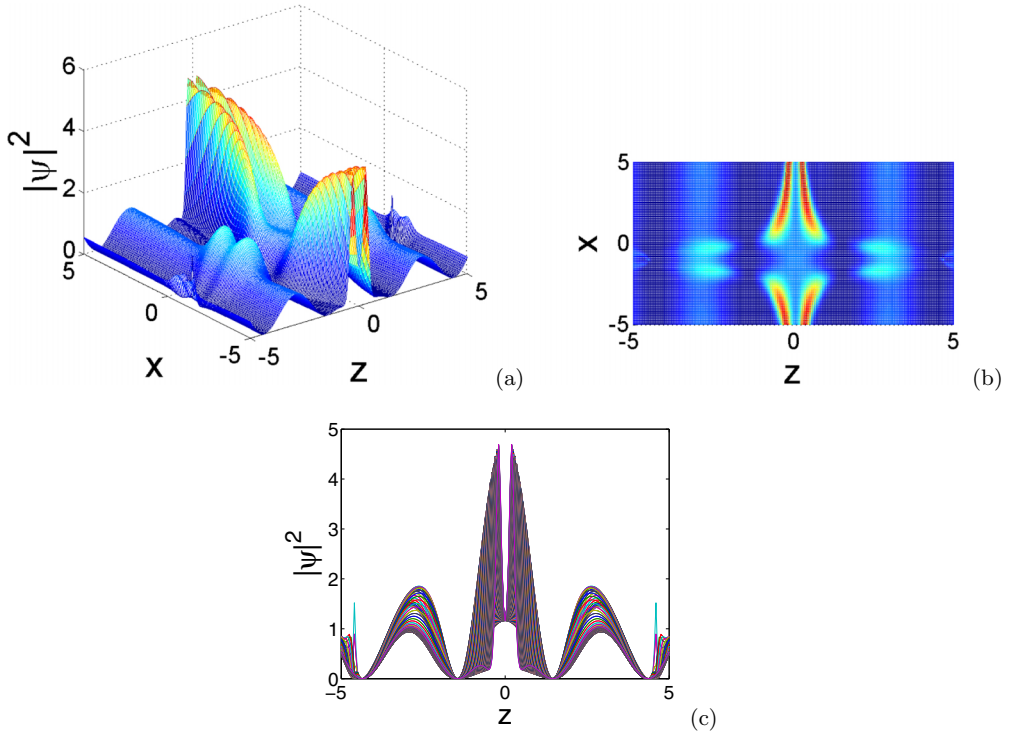

FIG. 6. (Color online) Wave propagation in 2D and 3D representations of the second-order rational solution for the intensity $|\psi_2(x,z)|^2$ with $d(z) = \mathrm{cn}(z,k)$, $p(z) = -\frac{1}{2}\mathrm{sn}(k,z)$, $\alpha(z) = z$, and $\delta(z) = z$.

z direction. The intensity profiles of the nonparaxial rogue waves given in Figs. 3(a) and 3(c) show how they are localized in the z direction (with z taken as the time parameter). These waves appear spontaneously and decrease rapidly as shown in previous works [9,26,53,54].

Having completed the first order, we now study the dynamic behavior of the nonparaxial effect on the propagation of nonparaxial rogue waves related to the second-order rational solutions. Here the parameters that were used to plot the first-order rational solutions are also used to obtain the intensity profiles of second order. So from Eq. (34) the nonparaxial effects on rogue waves are shown in 3D [Fig. 4(a)] and 2D [Figs. 4(b) and 4(c)] representations.

It follows from Eq. (35) that Fig. 5 reveals the nonparaxiality effect [Figs. 5(a) and 5(b)]. The intensity profiles of Figs. 4 and 5 are remarkably similar to Figs. 1 and 2. Nevertheless, we record a difference, particularly notable in the number of collisions and peaks near the periphery of the center.

In the same way, we use the Jacobian elliptic functions to plot the profiles of second order. By using Eq. (37) we obtain Figs. 6(a)–6(c), which show the influence of the nonparaxiality on rogue waves.

In Fig. 6 we observe many collisions between waves. We record again an unusual symmetry of the nonparaxial rogue waves in Fig. 6(a). The wave peak of Fig. 6(c) splits into two and this split is due to the diffraction effect in a lossy medium. We note that in the presence of the nonparaxiality, the collisions between waves are rare but significant when they appear [see Figs. 6(a) and 6(b)].

IV. CONCLUSION

In this work we have presented the first- and the second-order rational solutions related to the analytical rogue wave solutions. By using one direct method known as the similarity transformation and Darboux transformation, we have constructed the final rational solutions of the nonparaxial NLS equation by collecting partial solutions obtained from the standard NLS equation and the ones from the similarity reduction. This method can also be applied to the higher orders (third, fourth, etc.). Through the 2D and 3D representations we showed the effect of the nonparaxiality on the propagation of rogue waves: It follows that the nonparaxiality increases rapidly the intensity of rogue waves by increasing the length and reducing the width peak simultaneously. We noted that the nonparaxial rogue waves are faster than the ones obtained from the standard NLS equation. We have recorded that the nonparaxiality moves the higher peak of rogue waves from the center to the periphery. We also showed the effect of the polynomial and Jacobian elliptic functions on rogue waves. We concluded that the displacement of the wave peak from the center to the periphery is due to height velocity of the nonparaxial rogue waves. As the nonparaxial effect increases the velocity of waves, it also penalizes the interactions between them. These aspects are additional features and can find application in optics, notably in telecommunications, and in many other physical systems.

[1] A. Hasegawa and F. Tappert, Appl. Phys. Lett. **23**, 142 (1973).

[2] L. F. Mollenauer, R. H. Stolen, and J. P. Gordon, Phys. Rev. Lett. **45**, 1095 (1980).

[3] R. H. Stolen, L. F. Mollenauer, and W. J. Tomlison, Opt. Lett. **8**, 186 (1983).
[4] L. F. Mollenauer, R. H. Stolen, J. P. Gordon, and W. J. Tomlinson, Opt. Lett. **8**, 289 (1983).
[5] P. D. Miller and N. N. Akhmediev, Phys. Rev. E **53**, 4098 (1996).
[6] G. Baruch, G. Fibich, and S. Tsynkov, Opt. Express **16**, 13323 (2008).
[7] P. Chamorro-Posada, G. S. McDonald, and G. H. C. New, J. Mod. Opt. **45**, 1111 (1998).
[8] S. I. Fewo, H. Moussambi, and T. C. Kofane, Phys. Scr. **84**, 035002 (2011).
[9] Z. Yan, Phys. Lett. A **374**, 672 (2010).
[10] D. H. Peregrine, J. Aust. Math. Soc. Ser. B **25**, 16 (1983).
[11] Y. C. Ma, Stud. Appl. Math. **60**, 43 (1979).
[12] N. Akhmediev and V. I. Korneev, Theor. Math. Phys. **69**, 1089 (1986).
[13] N. Akhmediev, V. M. Eleonskii, and N. E. Kulagin, Theor. Math. Phys. **72**, 809 (1987).
[14] J. M. Dudley, G. Genty, F. Dias, B. Kibler, and N. Akhmediev, Opt. Express **17**, 21497 (2009).
[15] A. N. Ganshin, V. B. Efimov, G. V. Kolmakov, L. P. Mezhov-Deglin, and P. V. E. McClintock, Phys. Rev. Lett. **101**, 065303 (2008).
[16] A. N. W. Hone, J. Phys. A: Math. Gen. **30**, 7473 (1997).
[17] A. Montina, U. Bortolozzo, S. Residori, and F. T. Arecchi, Phys. Rev. Lett. **103**, 173901 (2009).
[18] P. Müller, C. Garrett, and A. Osborne, Oceanography **18**, 66 (2005).
[19] A. Nakamura and R. Hirota, J. Phys. Soc. Jpn. **54**, 491 (1985).
[20] M. Noumi and Y. Yamada, Nagoya Math. J. **153**, 53 (1999).
[21] D. R. Solli, C. Ropers, P. Koonath, and B. Jalali, Nature (London) **450**, 1054 (2007).
[22] M. Ballav and A. R. Chowdhury, Chaos **17**, 013102 (2007).
[23] Y. V. Bludov, V. V. Konotop, and N. Akhmediev, Phys. Rev. A **80**, 033610 (2009).
[24] L. Stenflo and M. Marklund, J. Plasma Phys. **76**, 293 (2010).
[25] Z. Yan, Commun. Theor. Phys. **54**, 947 (2010).
[26] N. Akhmediev, A. Ankiewicz, and J. M. Soto-Crespo, Phys. Rev. E **80**, 026601 (2009).
[27] J. Atangana, B. G. O. Essama, F. Biya-Motto, B. Mokhtari, N. C. Eddeqaqi, and T. C. Kofane, J. Mod. Opt. **62**, 392 (2015).
[28] B. G. O. Essama, J. Atangana, F. Biya-Motto, B. Mokhtari, N. C. Eddeqaqi, and T. C. Kofane, J. Mod. Opt. **61**, 1002 (2014).
[29] B. G. O. Essama, J. Atangana, B. M. Frederick, B. Mokhtari, N. C. Eddeqaqi, and T. C. Kofane, Phys. Rev. E **90**, 032911 (2014).
[30] W.-P. Zhong, M. R. Belic, and T. Huang, Phys. Rev. E **87**, 065201 (2013).
[31] B. G. O. Essama, J. Atangana, F. Biya-Motto, B. Mokhtari, N. C. Eddeqaqi, and T. C. Kofane, Opt. Commun. **331**, 334 (2014).
[32] D. R. Solli, C. Ropers, and B. Jalali, Phys. Rev. Lett. **101**, 233902 (2008).
[33] R. Y. Hao, L. Li, Z. H. Li, and G. S. Zhou, Phys. Rev. E **70**, 066603 (2004).
[34] J. F. Zhang, Q. Yang, and C. Q. Dai, Opt. Commun. **248**, 257 (2005).
[35] J. F. Wang *et al.*, Opt. Commun. **263**, 328 (2006).
[36] J. Li *et al.*, J. Phys. A: Math. Gen. **40**, 13299 (2007).
[37] K. Porsezian *et al.*, Phys. Lett. A **361**, 504 (2007).
[38] C. Q. Dai, G. Q. Zhou, and J. F. Zhang, Phys. Rev. E **85**, 016603 (2012).
[39] N. Akhmediev, A. Ankiewicz, and M. Taki, Phys. Lett. A **373**, 675 (2009).
[40] H. Wang and W. She, Opt. Commun. **245**, 145 (2005).
[41] F. Biancalana and C. Creatore, Opt. Express **16**, 14882 (2008).
[42] Z. Yan and C. Dai, J. Opt. **15**, 064012 (2013).
[43] S. Chen, L. Yi, D.-S. Guo, and P. Lu, Phys. Rev. E **72**, 016622 (2005).
[44] V. M. Pérez-García, P. J. Torres, and V. V. Konotop, Physica D **221**, 31 (2006).
[45] S. A. Ponomarenko and G. P. Agrawal, Phys. Rev. Lett. **97**, 013901 (2006).
[46] S. Kumar and A. Hasegawa, Opt. Lett. **22**, 372 (1997).
[47] Y. Ozeki and T. Inoue, Opt. Lett. **31**, 1606 (2006).
[48] E. N. Tsoy, A. Ankiewicz, and N. Akhmediev, Phys. Rev. E **73**, 036621 (2006).
[49] Yu. V. Bludov, V. V. Konotop, and N. Akhmediev, Eur. Phys. J. ST **185**, 169 (2010).
[50] A. T. Avelar, D. Bazeia, and W. B. Cardoso, Phys. Rev. E **79**, 025602 (2009).
[51] J. M. Soto-Crespo, Ph. Grelu, and N. Akhmediev, Phys. Rev. E **84**, 016604 (2011).
[52] P. F. Byrd and M. D. Friedman, *Handbook of Elliptic Integrals for Engineers and Scientists*, 2nd ed. (Springer, Berlin, 1971).
[53] P. Gaillard (unpublished).
[54] X.-L. Wang, W.-G. Zhang, B.-G. Zhai, and H.-Q. Zhang, Commun. Theor. Phys. **58**, 531 (2012).